Materials Today Sustainability 23 (2023) 100452

Contents lists available at ScienceDirect

Materials Today Sustainability

journal homepage: https://www.journals.elsevier.com/materials-today-sustainability

A diffusion-reaction computational study to reveal the depolymerization mechanisms of epoxy composites for recycling

C. Luo, C. Chung, K. Yu*

Department of Mechanical Engineering, University of Colorado Denver, Denver, CO 80217, USA

ARTICLE INFO

Article history:
Received 7 March 2023
Received in revised form
19 June 2023
Accepted 3 July 2023
Available online 12 July 2023

Keywords:
Bond exchange reactions
Transesterification
Epoxy depolymerization
Composite recycling
Finite element simulation

ABSTRACT

It has been recently discovered that the thermosetting matrix of engineering composites can be fully depolymerized in organic solvents through covalent bond exchange reactions (BERs) between the polymer network and solvent molecules. This breakthrough enables the eco-friendly and sustainable recovery of valuable fiber reinforcements using mild processing conditions. However, current investigations have been limited to proof-of-concept experimental demonstrations, leaving unanswered questions regarding the influence of temperature, solvent choice, and fiber arrangement on composite depolymerization performance. These factors are crucial for the commercialization and widespread industrial implementation of this technique. To address this significant knowledge gap, this study aims to establish the relationship between composite depolymerization speed and various material and processing conditions. A multiscale diffusion-reaction computational model is defined based on the finite element method, which links the microscale BER rate to the continuum-level composite depolymerization kinetics. Specifically, it reveals how the processing temperature, solvent diffusivity, fiber content, and fiber arrangement affect the overall composite depolymerization speed. The study enhances our understanding of the underlying mechanisms of composite recycling using organic solvents. As a result, it provides valuable insights for industrial stakeholders, allowing them to optimize depolymerization conditions, make informed material selections, and develop suitable business models for waste management.

© 2023 Elsevier Ltd. All rights reserved.

1. Introduction

Carbon fiber reinforced polymer (CFRP) composites have gained significant popularity in various high-performance engineering applications due to their outstanding mechanical strength, lightweight, chemical resistance, and stable thermomechanical properties [1,2]. However, the recycling of CFRP waste poses substantial challenges with conventional techniques, primarily because the matrix material is typically crosslinked with thermosetting polymers [3]. The recovery of valuable reinforcement carbon fibers from end-of-life CFRP materials holds great potential for promoting sustainable development and environmental protection. It has been reported that recycled carbon fibers can be obtained at approximately 70% of the cost of virgin carbon fibers. Moreover, compared to the production of new carbon fibers, the recycling process for these fibers significantly reduces emissions by 90%–95% and consumes 98% less energy [4–7].

Various reprocessing and recycling techniques have been investigated to reclaim carbon fibers from CFRP wastes. For example, mechanical recycling involves shredding CFRP scraps into small fragments that can be utilized as low value additives in other applications. Thermal or chemical reprocessing (e.g. pyrolysis, solvolysis, or fluidized bed) [8–14] uses energy-intensive processing conditions involving high temperature, pressure, and supercritical acids to decompose the polymer matrix and recover the embedded carbon fiber. While these techniques offer great benefits for sustainable development, and some of them are at the early stages of commercialization [15,16], they do have certain limitations, such as reduction in the mechanical strength and economic value of recycled fiber, or the requirements on harsh processing conditions that are not friendly to workers and larger-scale industrial applications.

Sustainable and environmentally friendly techniques have been emerged for the depolymerization of thermoset matrices by leveraging dynamic chemical reactions between solvents and

* Corresponding author.
E-mail address: kai.2.yu@ucdenver.edu (K. Yu).

https://doi.org/10.1016/j.mtsust.2023.100452
2589-2347/© 2023 Elsevier Ltd. All rights reserved.

polymers [17–29]. The thermoset matrix is shown to be fully depolymerized in a suitable organic solvent under mild processing conditions. Both depolymerized solution and reclaimed fibers can be reused to fabricate new CFRPs. One notable approach utilizes dynamic bond exchange reactions (BERs), wherein the choice of solvent and catalyst depends on the specific covalent bonds targeted on the chain backbone of the thermoset matrix. For example, composites containing dynamic disulfide linkages can be decomposed using thiol-containing solvents [30–32], while polyimine composites with imine exchangeable bonds can be degraded in diamine solvents [33–36]. Furthermore, epoxy thermosets with ester groups on the chain backbone can be depolymerized in alcohol solvents through transesterification BERs [37–43] (see Fig. 1). An exciting aspect of these BER-based techniques is their reversibility. After depolymerization, the resulting polymer solution can be re-polymerized by heating it in an open environment to evaporate the alcohol solvent. The recycled epoxy exhibits a network structure and mechanical properties that are nearly identical to the original material. Compared to existing methods, this solvent-assisted recycling method offers several advantages, including easy implementation, minimal pollution, and retention of mechanical strength through simple heating in low-toxic organic solvents.

Despite the exciting technological innovations, there is a high demand for a fundamental study on the influences of various materials and process conditions on the matrix depolymerization process, which plays a critical role in the development of economically viable business models and the design of supply chains for waste materials in large-scale engineering applications.

Due to the nascent development of the depolymerization technique, existing studies have primarily focused on proof-of-concept demonstrations involving various material systems, solvents, and catalyst choices. However, there is still a lack of detailed understanding regarding the material-process-depolymerization relationships specifically pertaining to polymer composites. In our previous studies [44], the relationships between microscale dynamic reaction kinetics and macroscale depolymerization behaviors of pure thermoset matrix are investigated using a one-dimensional constitutive model. However, the influencing mechanisms of carbon fiber, particularly the fiber arrangement, aggregates, and volume content, on the solvent transportation and matrix depolymerization kinetics remain unknown. For example, with more carbon fiber presents in the composites, there is less amount of matrix in the material system, thus requiring less amount of solvent or catalyst to fully depolymerize the thermosetting polymer and reclaim the carbon fiber. On the other hand, the individual fiber blocks the contact between the solvent and polymer matrix, as well as the transportation pathway of solvent and catalyst, which might reduce the overall depolymerization speed at equivalent processing temperatures.

To quantitatively analyze this complex process, we develop a multiscale diffusion-reaction finite element computational model to investigate the depolymerization performance of epoxy composites. The model links the microscale chemical reaction kinetics to the macroscope depolymerization degree under different material and processing conditions, including the fiber volume fraction, fiber aggregates, processing temperature, and solvent diffusivity. The computational model is shown to closely capture the experimental characterization results. It is further employed in parametric studies to reveal the material-process-depolymerization relationships and influencing mechanisms of various processing parameters. The study reveals depolymerization domains for epoxy composites that are respectively dominated by BER kinetics and solvent diffusivity. The fundamental understanding will pave the way for the practical implementation of these techniques in real-world scenarios, contributing to the advancement of environmentally friendly and economically viable CFRP recycling practices.

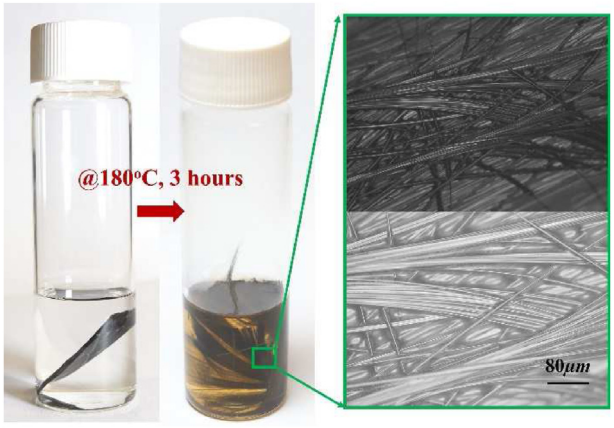

Fig. 1. Experimental demonstration showing the epoxy composites can be fully depolymerized in the ethylene glycol solvent at mild processing temperatures. Clean fibers can be reclaimed without damage. Note: The two microscopic images depict the same recycled fiber bundle, captured at different locations, and presented with varying contrasts to emphasize microscale details.

2. Material and experiments

2.1. Material preparations

In this study, an anhydride-cured thermosetting epoxy is selected as the matrix material. It was prepared using commercially available chemicals, including the epoxy monomer Bisphenol A diglycidyl ether (DGEBA, M_w = 340 g/mol) and the crosslinking agent hexahydro-4-methylphthalic anhydride (M_w = 168 g/mol). 2,4,6-tris (dimethylaminomethyl) phenol was used as the polymerization accelerator. All chemicals were purchased from Sigma Aldrich (St. Louis, MO) without requiring further purification. During the material synthesis, the mole ratio between the epoxy monomer and anhydride crosslinker was 1:1. The weight ratio between the epoxy monomer and accelerator was 10:0.1. After mixing the precursor chemicals, the liquid mixture was poured into a mold and placed in an oven for 2 h at 100 °C. Finally, the temperature was increased to 150 °C for an additional 2 h.

Epoxy composites were fabricated using the hand lay-up procedure followed by the vacuum bagging process. Unidirectional carbon fiber fabric (FibreGlast Inc., Brookville, OH) was used as reinforcements. Composite lamina samples with 19%, 33%, and 40% fiber volume fractions were prepared by mixing the epoxy resin and fiber at the designated ratios. The lay-up was vacuum-bagged and was left to cure using the above-mentioned thermal temporal conditions.

The mechanical properties of the fabricated epoxy thermosets and their composites with 19% carbon fiber were examined using room-temperature uniaxial tension tests. The detailed results of these tests can be found in the Supplementary Materials (Section S1). It is observed that both epoxy samples and the composite samples exhibit outstanding mechanical stiffness and strength, making them suitable for various demanding engineering applications.

2.2. Thermomechanical properties of epoxy matrix

The glass transition behavior of the epoxy matrix was tested using a dynamic mechanical analysis (DMA, Model Q800, TA Instruments, New Castle, DE). The epoxy samples were cut to the

same dimensions of 16 mm × 5 mm × 0.6 mm. Prior to the tests, the samples were equilibrated at a temperature of 23 °C for a duration of 10 min to ensure thermal stability. During the DMA tests, the strain on the samples was oscillated at a frequency of 1 Hz with a peak-to-peak amplitude of 0.1%. Simultaneously, the temperature was increased from 23 °C to 200 °C at a constant rate of 2 °C/min.

2.3. Swelling and depolymerization measurements

Ethylene glycol (EG, Sigma Aldrich) solvent is used to enable the depolymerization of epoxy. Since the anhydride-cured epoxy samples contain ester bonds on the chain backbone, they can be fully depolymerized in EG solvent mixed with the transesterification catalyst triazabicyclodecene (TBD, Sigma Aldrich). Without the catalyst, the epoxy network cannot be depolymerized, but instead, it will continue to swell until it reaches an equilibrium state within the EG solvent. It is worth noting that the tertiary amine groups present in the polymerization accelerator, 2,4,6-tris(dimethylaminomethyl)phenol, have been shown in recent works [45,46] to potentially act as catalysts for transesterification reactions. However, as will be shown in Section 4.1, after immersing the epoxy networks in the pure EG solvent for 10 h, there is no significant change in the appearance of the samples. The tertiary amine groups in the accelerator did not exhibit a notable effect in promoting transesterification reactions or enabling network depolymerization. This might be attributed to either the relatively low content of the accelerator (1%) or the relatively low swelling temperature of 140 °C. Therefore, the potential catalyst effect is not considered in this study.

Gravimetric swelling measurements were conducted to evaluate the diffusion rate of solvent in the epoxy matrix with different configurations. Epoxy samples were immersed in the solvent (without TBD catalyst) at constant temperatures, and their mass increments were recorded at specific time intervals.

To measure the depolymerization speed, epoxy samples were prepared with different configurations and then soaked in EG solvent mixed with 0.3 mol/L TBD catalyst. The provided solvent amount is more than sufficient to fully depolymerize the epoxy networks. The quantity of solvent provided was more than sufficient to ensure the complete depolymerization of the epoxy networks. To prevent solvent evaporation, the glass dish was covered with a glass slide and placed in a heating oven at a constant temperature for depolymerization. At specific time intervals, the epoxy sample was carefully removed from the solvent, wiped to remove any excess solvent, and placed on a scale to measure its weight. The complete depolymerization of the epoxy network was determined by the absence of solids in the solvent.

After fully depolymerizing the epoxy matrix, the excess EG solvent present in the solution can be separated and recycled for subsequent operations, thereby minimizing waste generation and environmental pollution. For instance, upon cooling the solution to room temperature, a distinct phase separation occurs between the depolymerized epoxy oligomers and the excess EG solvent. This phenomenon has been demonstrated in our previous study on a similar epoxy network [37], as well as in the previous work conducted by Kuang et al. [47] on the same epoxy network. Additionally, the EG solvent can undergo further purification through the solvent distillation method.

The depolymerization speeds of composites with different fiber contents were measured in the same way. It is noted that the adopted unidirectional fiber fabric is held together by fill threads in the transverse direction, which remained intact during the depolymerization process. The depolymerization speed was characterized by the composite weight, which includes the weight of the fiber fabric and the residual epoxy matrix adhered to the fabric.

3. Finite element computational modeling for composite depolymerization

3.1. Overall modeling framework

Fig. 2a shows the network structure of the prepared anhydride-cured epoxy, which highlights ester groups on the chain backbone. The detailed network depolymerization mechanisms under the action of alcohol solvent is presented in the Supplementary Material (Section S2). Based on the depolymerization mechanism, the overall computational modeling framework of the composite depolymerization is shown in Fig. 2b–g. In this study, we conducted depolymerization tests on thin-film lamina composite samples with a dimension of 100 mm in length, 30 mm in width, and 1.6 mm in thickness. The length of the composite lamina samples is significantly larger than the average cross-section size. When these composite samples are immersed in EG solvent, the depolymerization process primarily occurs on the top and bottom surfaces, while depolymerization along the length direction is relatively less significant due to the smaller contact area. In this manner, the depolymerization process is taken to be a 2D plane-strain diffusion-reaction problem (Fig. 2b). However, it is important to note that this assumption may not fully capture the depolymerization behavior of composite laminates in a real-scale 3D scenario. The depolymerization process in composite laminates could be influenced by neighboring laminas, given the heterogeneity of fiber-reinforced composites. For a comprehensive understanding of depolymerization in such cases, full-scale 3D simulations should be considered.

Within the modeling framework, the individual fiber is assumed to have no reaction with solvent molecules, and its location is fixed in the computational model. When immersing the sample in EG solvent mixed with TBD catalyst, both two constituents diffuse into the network. At the microscale view (Fig. 2g), the transesterification reactions between EG molecules and ester bonds lead to chain cleavage of the backbone. Note that depending on the content of reactive solvent molecules, the cleaved chain segments may reconnect *via* transesterifications, with free solvent molecules produced as a by-product. When a sufficient quantity of solvent is supplied, the system equilibrium tends to favor the depolymerization of the epoxy network, and the epoxy sample gradually breaks into soluble oligomers (Fig. 2f). On the polymer-solvent interface (Fig. 2e and d), the cleaved chain segments disentangle from the network at a rate that scales with the segment length. The interface between the solvent and polymer matrix moves as the depolymerization proceeds (Fig. 2c). The overall network depolymerization rate is therefore determined by the rates of three time-dependent processes: i) the diffusion of solvent and catalyst molecules, ii) the cleavage and reconnection of chain segments, and iii) the disentanglement rate of chain segments. The following sections detail the kinetics of each process, as well as their governing equations and modeling approaches.

3.2. Kinetics of composite matrix depolymerization

Process 1 - Continuum-level Solvent and Catalyst Transportation: Tremendous studies have been performed to solve the diffusion-reaction problem using FEA simulations [48–52]. In this study, we focus on finding a simple yet effective modeling framework to capture the essential experimental data and use it to reveal the influencing mechanisms of different materials and process conditions on the composite depolymerization kinetics. To this end, two fundamental assumptions are made. First, we assume that the impact of the stress field on diffusion and

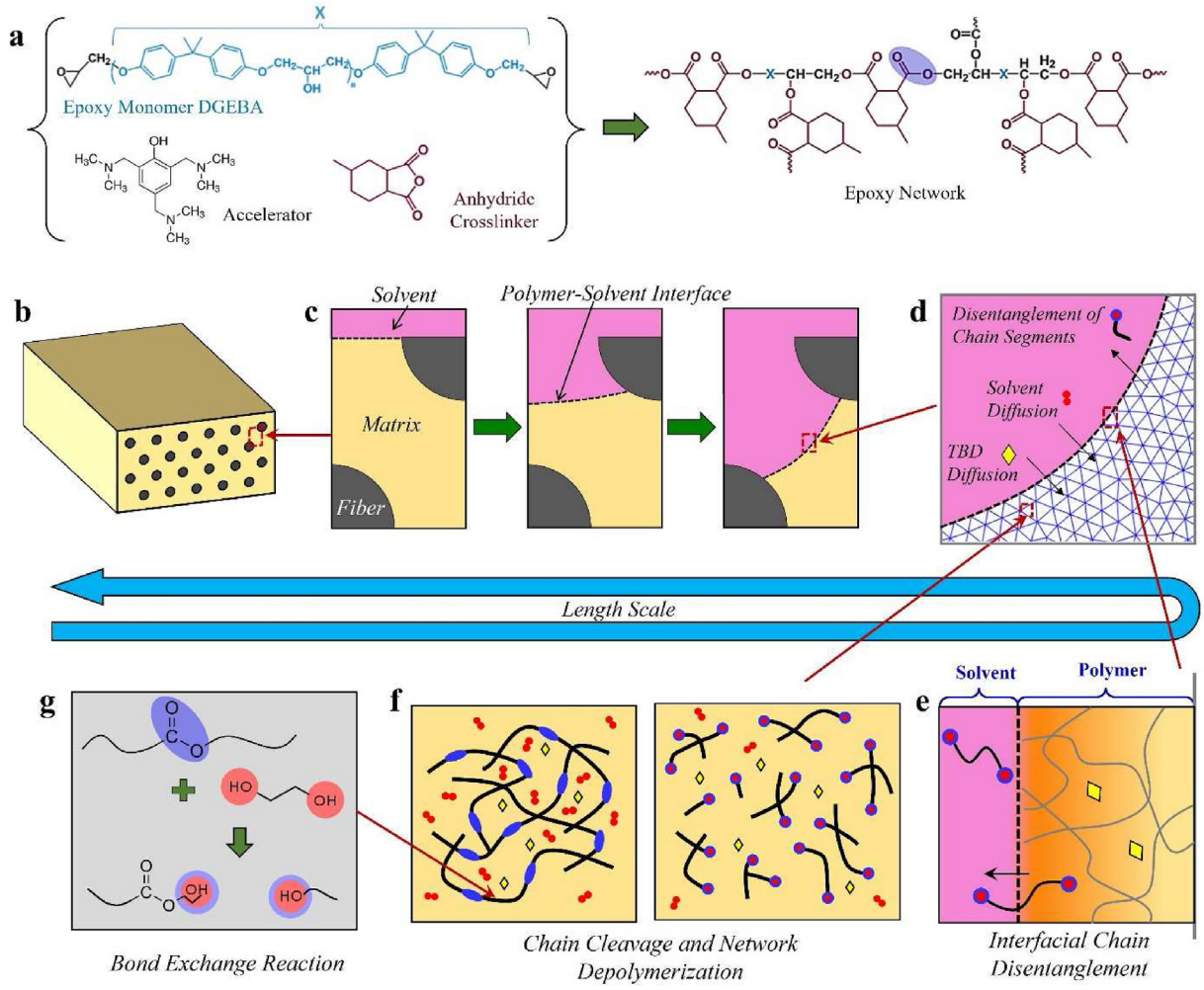

Fig. 2. **(a)** The molecular network structure of the synthesized epoxy sample with an ester bond highlighted on the chain backbone. **(b)** The continuum-level composite lamina sample with continuous carbon fiber. **(c)** The movement of the composite-solvent interface as the depolymerization proceeds. **(d)** The mesoscale FEA model. Around the composite-solvent interface, solvent and catalyst molecules diffuse into the matrix network, and the cleaved chain segments diffuse out of the network. **(e)** The disentanglement of the chain segments around the interface. **(f)** The network depolymerization. **(g)** The microscale transesterifications between alcohol and ester bonds lead to chain cleavage.

reaction kinetics within the polymer network is neglected. This assumption was based on the understanding that the highly crosslinked epoxy matrix exhibits a minimal swelling ratio and hydrostatic pressure, rendering the stress field's influence negligible. Second, we disregarded the diffusion of cleaved chain segments within the network since it is overshadowed by the transportation of solvent molecules. Instead, we considered the chain segments to be disentangled from the polymer-solvent interface, thereby serving as a boundary condition for the internal variables.

The global balance of solvent transportation is written in the integral form as:

$$\int_{\Omega_R} \frac{\partial C_s}{\partial t} dv = -\int_{\partial\Omega_R} \boldsymbol{j}_s \cdot \boldsymbol{n} da + \int_{\Omega_R} k_s dv \tag{1a}$$

where dv is an infinitesimal volume element, da is an infinitesimal area on the polymer-solvent interface, $\mathbf{n}$ is the unit vector normal to the interface, $C_s(x,t)$ (mol/m^3) is the solvent volumetric mole content, $\boldsymbol{j}$ is the surface flux of solvent, k_s (x_1, x_2, x_3) is the volumetric changing rate of alcohol solvent content due to the transesterification BERs. Assuming the Fickian diffusion, the surface flux of the solvent can be related to the solvent diffusivity D_s as: $\boldsymbol{j_s} = -D_s \nabla C_s$.

In the local form for an arbitrary control volume, the transportation equations can be rewritten as a partial differential equation as:

$$\frac{\partial C_s}{\partial t} = \nabla \cdot (D_s \nabla C_s) + k_s \tag{1b}$$

The solvent diffusivity D_s (in Eq. (1)) within a polymer network increases with the temperature following the well-established Arrhenius law. The diffusivity also increases at a lower network crosslinking density because more free volume among macromolecular chains is available for solvent transportation [53–60]. To represent the decrease of network crosslinking density during the recycling process, we define the network depolymerization degree p. This scalar variable ranges from 0 to 1 and represents the overall macroscopic depolymerization degree of the sample. Its detailed formulation depends on the degree of BERs and will be introduced in the following section. As found in previous studies [61–63], D_s is scaled to the depolymerization degree as $D_s \sim exp(\delta p^{\xi})$, where δ and ξ are the fitting parameters. Based on these considerations, the solvent diffusivity during the composite depolymerization is written as:

$$D_s = \underbrace{D_{s0}(T_0)}_{\substack{\text{Reference}\\ \text{Diffusivity}}} \underbrace{\exp\left[-\frac{E_s}{R}\left(\frac{1}{T}-\frac{1}{T_0}\right)\right]}_{\text{Temperature}} \underbrace{\exp[\delta(p^{\xi}-1)]}_{\substack{\text{Depolymerization}\\ \text{Degree}}} \quad (2)$$

wherein D_{s0} is the solvent diffusivity of the as-fabricated epoxy ($p = 0$) at a reference temperature T_0. E_s is the activation energy for solvent diffusion. R=8.31 J/mol/K is the gas constant.

It is important to note that in this study, the transesterification catalyst for the base-catalyzed epoxy ring-opening (BER) reaction is considered a solute. The catalyst is carried into the epoxy network by the solvent during the depolymerization of the composite. The content of the catalyst within the composite matrix is assumed to be identical to that in the external solvent mixture.

Process 2 – Microscale Analysis on the Kinetics of Chain Cleavage: In the above continuum-level modeling framework, the formulations of the changing rate of solvent content, k_s, and the depolymerization degree at a given material point, p, require the microscale statistical analysis on the BERs between solvent molecules and the chain segments with different lengths.

Based on the contents and average distance of solvent molecules and chain segments, the rates of chain cleavage (k_1) and connection (k_2) during the network depolymerization are determined for a given material point. For the chain cleavage reaction, the solvent molecules first diffuse towards an ester bond on the chain backbone and then break the chain *via* BER. The reaction rate k_1 (mol/s) for the chain cleavage can be written as:

$$k_1 = (N_A t_1 + N_A t_{BER})^{-1} \quad (3a)$$

where t_1 is the traveling time of the solvent molecule. $t_1 = \langle r_1\rangle^2/D_s$, with $\langle r_1\rangle$ being the average distance between an ester bond and hydroxyl group. According to the theory of mean interparticle distance, $\langle r_1\rangle = a\Gamma(1/3)/3$, where Γ is the gamma function. $a = \sqrt[3]{4N_A\pi C_s/3}$ is the Wigner-Seitz radius. N_A is the Avogadro's number (6.02×10^{23} mol). t_{BER} is the average time spent on a BER. $t_{BER} = t_{0\_BER}\, exp\,(E_{ab}/RT)$, with E_{ab} being the BER energy barrier, t_{0_BER} being a time constant, and T being the temperature in Kelvins.

For the chain connection, the chain segments first diffuse towards another reactive site and then connect *via* BER. The reaction rate k_2 (mol/s) for the chain connection can be written as:

$$k_2 = (N_A t_2 + N_A t_{BER})^{-1} \quad (3b)$$

where t_2 is the traveling time of a segment with i monomers to meet another reactive site at segment tails. Following our previous work [64], it can be formulated based on the relative distance and the diffusivity of chain segments. $t_2 = \tau_i(C_r N_A b^3)^{-4/3}$, with C_r being the concentration of exchangeable bonds at the segment tails at a continuum point, which is two times the content of the chain segment. b is the monomer length. τ_i is the Rouse time of the segment i monomers. If the Rouse time of the shortest segment at a reference temperature is τ_{0s}, the Rouse time of the segment with i monomers will be $\tau_{0i} = i^2\tau_{0s}\alpha(T)$ [64]. $\alpha(T)$ is the shift factor for the time-temperature superposition principle.

The rate constants are then used in first-order reaction equations to formulate the content and length distribution of chain segments during depolymerization. There are four types of BERs that will change the content of the segment with i monomers (i.e. C_i). As illustrated in Fig. S3 (Supplementary Materials), the four reactions are: (a) a segment with i monomers reacts with an EG molecule and breaks into two shorter segments; (b) a segment with i monomers reacts with another chain segment to form a longer chain segment and generate a new EG molecule; (c) two short chain segments react to form a segment with i monomers and generate a new EG molecule; (d) a long chain segment react with an EG to form a segment with i monomers and another chain segment. As shown in the following equation, at time t of depolymerization, the changing rate of chain segment content, C_i, is the summation of the reaction rates of the four reactions. Detailed derivations of the reaction rate can be found in our previous study [65].

$$\dot{C}_i = \underbrace{-k_2C_i}_{r_i^a} \underbrace{-k_1C_i}_{r_i^b} + \underbrace{k_1\sum_{j=1}^{i-1}C_j\left(C_{i-j}\Big/\sum_m C_m\right)}_{r_i^c} + \underbrace{k_2\sum_{j=i+1}C_j(2/(j-1))}_{r_i^d} \quad (4)$$

The reaction rates of four possible reactions in Fig. S3 also determine the changing rate of solvent content (C_s) at a material point mentioned in Eq. (1):

$$k_s(x_1,x_2,x_3,t) = \sum_{i=1}^{N}\left(r_i^a - r_i^b + r_i^c - r_i^d\right) \quad (5)$$

where N is the number of monomers along the chain backbone in the unprocessed epoxy sample.

Solving the above differential equations will determine the volumetric contents of chain segments with a length i, C_i, as well as the content of solvent molecules, C_s. since each segment i has i-1 ester bonds on the chain backbone, the content of ester bonds at a given material point is written as $\sum_{i=2}(i-1)C_i$. The average length chain segment is $L_{ave} = \sum_{i=2}iC_i/\sum_{i=2}C_i$. The network depolymerization degree is defined to be the amount of ester groups on the segment backbone, normalized by its initial value in the fully polymerized network:

$$p(t) = \frac{N\sum_{i=2}(i-1)C_i(t)}{(N-1)C_1(t=0)} \quad (6)$$

Process 3 - Disentanglement of Chain Segment and Composite Mass Loss: After the polymer chains are cleaved into short segments, they disentangle from the epoxy network at the polymer-solvent interface and diffuse into the solvent. According to the reputation theory [66,67], the segment disentanglement rate, k_{di} (mol/m^3s), is scaled to the segment length and is formatted as:

$$k_{di} = \alpha_d\frac{C_i}{\tau_i} \quad (7a)$$

where α_d is a unitless scaling factor. τ_i is the Rouse time (Eq. (3b)) of segments with i monomers.

After the disentanglement, the transportation of chain segments in the depolymerization solvent is also diffusion driven. In this study, there are more than sufficient solvents provided to depolymerize the epoxy and composites (the amount of solvent is ten times greater than the amount of epoxy material). Therefore, the disentangled chain segments are quickly diluted within the solvent and their diffusion time scale plays a negligible role in determining the overall composite depolymerization speed. Based on these considerations, the mass loss of epoxy and composite samples during the depolymerization is formulated as:

$$\dot{m} = \sum_{i=1}^{N}\frac{i}{N}k_{di}p_e \quad (7b)$$

where p_e is the average mole mass of polymer chains between two successive crosslinkers of the as-fabricated epoxy samples.

3.3. Finite element modeling approach

The diffusion partial differential equations (Eqs. (1) and (2)) are solved using a customized finite element code in MATLAB with 2D triangular elements. The solvent content at the finite element nodes is represented by the vector $\boldsymbol{d} = [C_{s1}(x_1, x_2, x_3), \ldots C_{sn}(x_1, x_2, x_3)]$, with n being the number of nodes in each element. The element governing equation is written as:

$$\boldsymbol{k_G}\dot{\boldsymbol{d}} + \boldsymbol{k_D}\boldsymbol{d} = \boldsymbol{r_s} \tag{8a}$$

$$\text{with } \boldsymbol{k_G} = \iiint_V \boldsymbol{N}\boldsymbol{N}^T dV, \boldsymbol{k_D} = \iiint_V \boldsymbol{B}\boldsymbol{D}\boldsymbol{B}^T dV, \text{and } \boldsymbol{r_s} = \iiint_V k_s \boldsymbol{N} dV \tag{8b}$$

in the above equations, $\boldsymbol{N} = [N_1(x_1, x_2, x_3), \ldots N_n(x_1, x_2, x_3)]$ is the shape function of the adopted finite elements. $\boldsymbol{B}$ is the element shape matrix with $B_{ij} = \partial N_i / \partial x_j$. $\boldsymbol{D}$ is the diffusivity matrix. With the assumption of isotropic materials, we have $D_{ij} = D_s \delta_{ij}$.

During the composite depolymerization, there is excessive solvent provided. Therefore, we assume the concentration of solvent molecules in the recycling solution is relatively constant. This imposes a Dirichlet-type essential boundary condition on the polymer-solvent interfaces:

$$C_s(x_1, x_2, x_3)|_{\partial\Omega_R} = C_s^0 \tag{9}$$

with C_s being the mole number of molecules of the pure EG solvent.

During the numerical analysis, the solvent contents of each element are first calculated based on Eq. (1). The chain segment contents are then updated based on the microscale reaction kinetics equations (Eqs. (4) and (5)), which are used as input for the next numerical step. The average segment length and the depolymerization degree (Eq. (6)) of each finite element are calculated and stored as internal variables. The segment disentanglement and mass loss (Eq. (7b)) are only for the elements on the polymer-solvent interfaces. Once the chain density of the boundary elements reaches zero, the elements are deactivated from the FEA model to update the position of polymer-solvent interfaces.

4. Results and discussion

4.1. Material parameters identification methods

At the continuum level, the solvent diffusivity within the epoxy network is one of the most significant parameters determining the composite overall depolymerization speed. The detailed model parameters can be determined using swelling tests of epoxy samples, which will be elaborated in detail in Section 4.2. The diffusivity also increases with the network depolymerization degree, p. Following our study on a similar epoxy network [68], the fitting diffusivity parameters δ and ξ were determined to be 3.1 and 0.3, respectively.

At the microscale chain cleavage and reconnections, E_{ab} is the BER energy barrier, and t_{0_BER} is a time constant. In our previous study [41], these two parameters were determined using a group of stress relaxation tests of epoxy samples at different temperatures, which gave $E_{ab} = 8.15$ kJ/mol, and $t_{0\_BER} = 2.3 \times 10^{-2}$ s. The Rouse time of the shortest segment $\tau_{0s} = 1$ min, and the monomer length $b = 1$ nm. Other material constants, such as the number of monomers between two crosslinkers, N, and Mole mass of polymer chains between two crosslinkers, p_e can be determined by the network thermomechanical properties as shown in Section 4.2.

For the disentanglement of chain segments of network depolymerization, α_d is a scaling factor for the disentanglement rate. It is determined by fitting with the experimental data of epoxy depolymerization rate, which will be described in Section 4.3.

All the material parameters involved in the modeling framework are listed in Table 1.

4.2. Diffusion of solvent within the epoxy matrix

The storage moduli and tan δ of the epoxy sample are shown in Fig. 3a. The temperature corresponding to the peak of the tan δ curve is taken to be the network glass transition temperature (T_g), which is 132 °C. The room-temperature modulus of the epoxy sample is ~1.8 GPa. The epoxy rubbery modulus (E_{eq}) at ~200 °C, which is an indicator of network crosslinking density, is ~23 MPa. It can be related to the molecular weight between two successive crosslinkers, p_e (in Eq. (7b)), as $E_{eq} = 3\rho RT/p_e$, with ρ being the polymer density. After calculation, p_e is ~5130 g/mol. On the other

Table 1
All the material parameters in the modeling framework.

Parameters	Values	Description
Continuum-level solvent diffusivity		
T_0	140 °C	The reference temperature for solvent diffusion
D_{s0}	5.5×10^{-4} mm^2/s	The reference solvent diffusivity
E_s	93 kJ/mol	The activation energy for solvent diffusion
δ	3.1	A fitting parameter for the influence of depolymerization degree
ξ	0.3	A fitting parameter for the influence of depolymerization degree
ρ	1 g/m^3	Density of the epoxy network
Microscale chain cleavage and reconnections		
b	1 nm	The average length of monomers
t_{0_BER}	2.3×10^{-2} s	A time constant for BERs
E_{ab}	8.15 kJ/mol	The energy barrier for BERs
τ_{0s}	60 s	The Rouse time of the shortest chain segment
c_1	3.7	The WLF equation parameter
c_2	21.5 °C	The WLF equation parameter
T_{t0}	30 °C	The reference temperature of the WLF equation
N	20	Number of monomers between two crosslinkers
Microscale chain disentanglement		
α_d	0.049	A fitting parameter for segment disentanglement rate
p_e	5130 g/mol	Mole mass of polymer chains between two crosslinkers

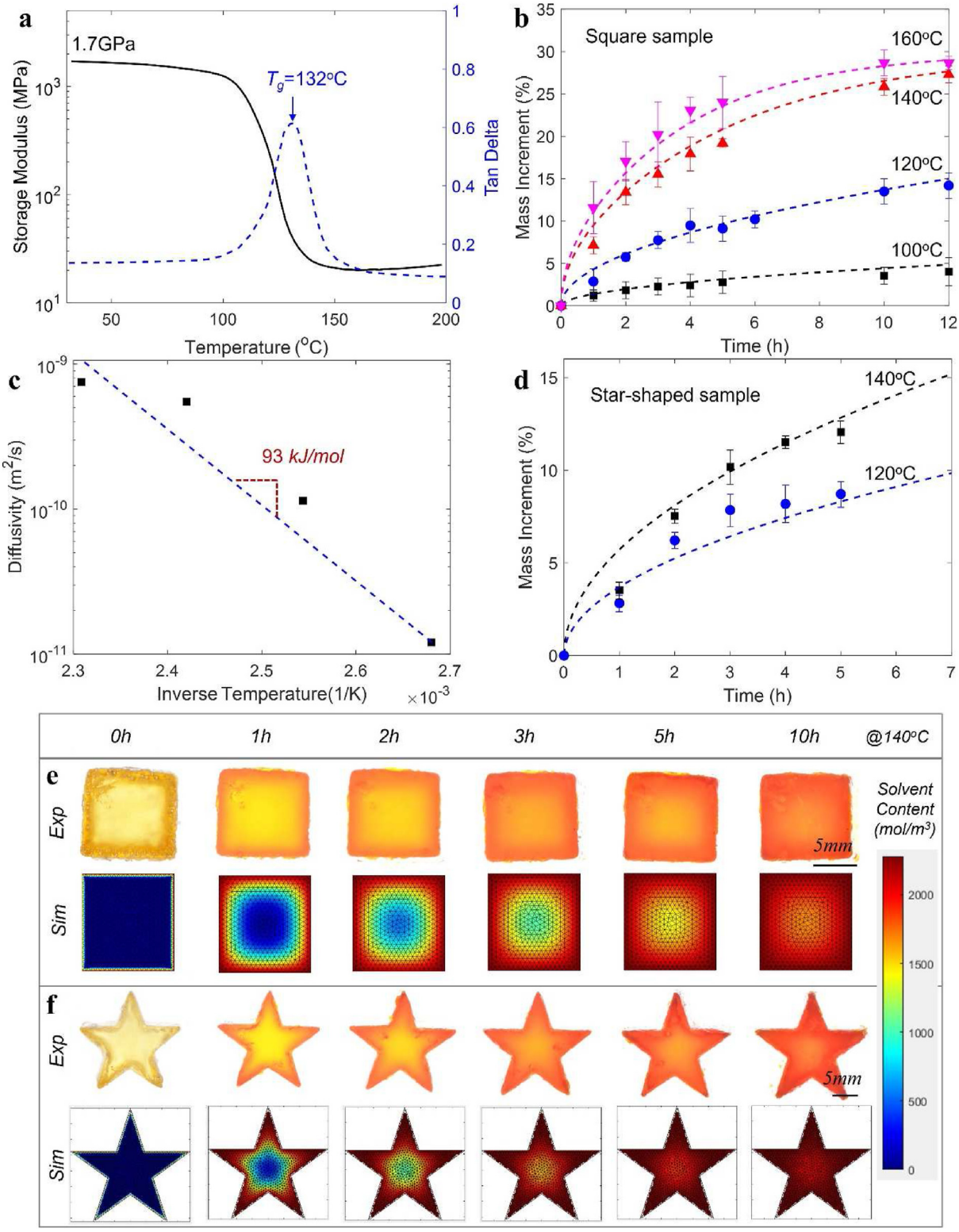

Fig. 3. **(a)** DMA tests of storage modulus and tan delta of the prepared epoxy sample. **(b)** Mass increment of cylindrical samples with a squared cross-section as a function of swelling time. The different curves in each figure correspond to variations in temperature. Dots: experimental data. Dashed lines: simulation results. **(c)** Solvent diffusivity as a function of the inverse Kelvin temperature. **(d)** Mass increment of cylindrical samples with a star-shaped cross-section as a function of the swelling time. Dots: experimental data. Dashed lines: simulation results. **(e)** and **(f):** Cross-section appearances of the squared and star-shaped epoxy samples in experiments (top row) and FEA simulations (bottom row).

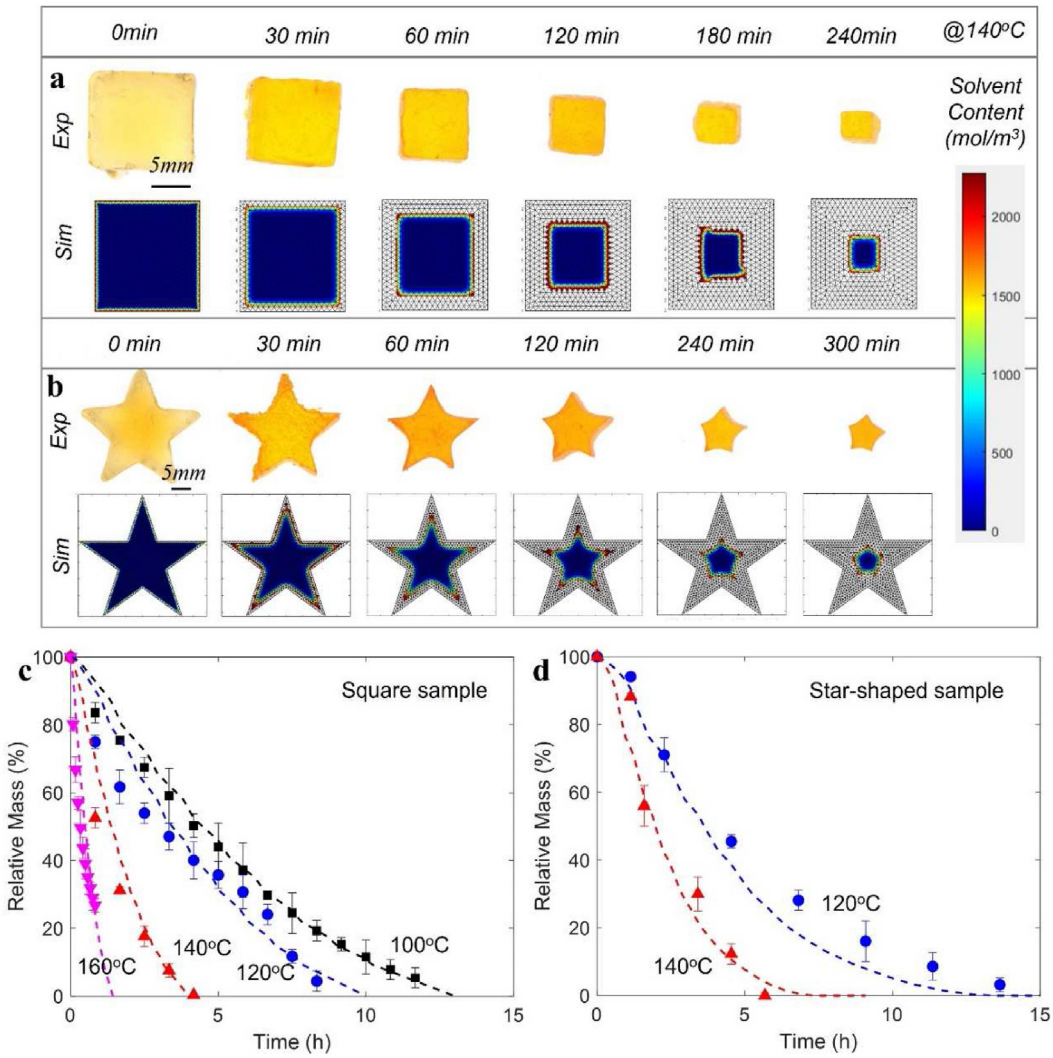

Fig. 4. Cross-sectional appearances of the **(a)** samples with a squared cross-section and **(b)** samples with a star-shaped cross-section in experiments (top row) and simulations (bottom row) during the depolymerization tests at 140 °C. Mass decrease of the **(c)** squared epoxy sample and **(d)** star-shaped epoxy samples as a function of depolymerization time and temperature. Dots: experimental data. Dashed lines: simulation results.

hand, the epoxy network was prepared using DGEBA ($M_w = 340$ g/mol) and the anhydride crosslinker ($M_w = 168$ g/mol) at a mole ratio of 1:1. The average molecular weight of the epoxy sample is 254 g/mol. Therefore, the number of monomers between two crosslinkers $N = 5130$ g/mol/254 g/mol ≈ 20.

The model parameters for solvent diffusivity in Eq. (2) are determined using the swelling tests on epoxy samples at different temperatures (100 °C, 120 °C, 140 °C, and 160 °C, respectively). Cylindrical samples with a squared cross-section were first fabricated with the identical cross-sectional dimensions (11 mm × 11 mm). The sample length (65 mm) is much greater than the size of the cross-section, so it can be treated as a 2D diffusion problem. The square epoxy samples were immersed in 20 g EG solvent in a flask. No BER catalyst was added to the solvent, so the samples swelled with no depolymerization. The mass increment of the samples was recorded to calculate the solvent diffusivity. The dots in Fig. 3b show the experimental results of the mass increment as a function of swelling time. The appearances of the sample cross-section at different stages of the soaking at 140 °C are shown in Fig. 3e. Note that in the pictures, the color of the sample gradually changes during the swelling processes. This is because Sudan I (Sigma Aldrich) was added into the EG solvent when we performed diffusion tests. It served as the dye to indicate the transportation and propagation frontline of solvent within the epoxy sample.

The established FEA model was used to predict the swelling mass of cubic samples by turning off the BERs within the modeling framework. By fitting with the experimental data at different temperatures in Fig. 3b (solid lines in the figure), the diffusivities are determined and are plotted in Fig. 3c as a function of inverse Kelvin temperature. The reference diffusivity at 140 °C $D_{s0} = 5.5 \times 10^{-4}$ mm^2/s. The activation energy for diffusion (E_s in Eq. (2)) $E_s = 93$ kJ/mol.

With the determined model parameters, the established FEA model was used to predict the diffusion of EG solvent in cylindrical samples with a star-shaped cross-section (65 mm length) with non-uniform solvent transportation. The corresponding mass increment of the sample at 120 °C and 140 °C are presented in Fig. 3d. The experimental pictures and simulations of the sample appearances at different stages of the soaking at 140 °C are compared in Fig. 3e. The results show that the simulations are reasonably close to the experimental data.

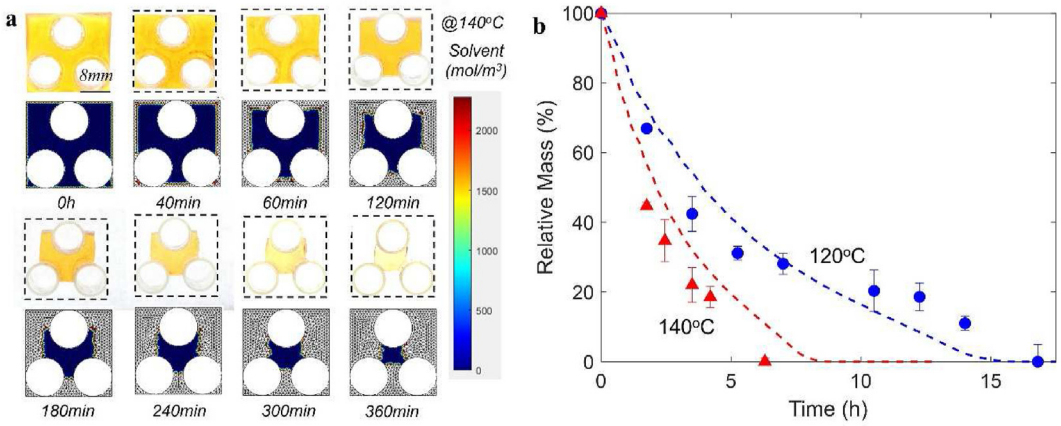

Fig. 5. **(a)** Cross-section appearances of the epoxy material structure with glass rods in experiments (top row) and simulations (bottom row) during the depolymerization tests at 140 °C. **(b)** Mass decreases of the material structure as a function of time. Dots denote experimental data. Dashed lines denote model predictions.

4.3. Depolymerization speed of the epoxy matrix

To characterize the epoxy depolymerization speed and determine the associated model parameters, cylindrical samples with a squared cross-section (~11 mm side length) were soaked in 20 g EG solvent mixed with 0.3 mol/L TBD catalysts. The appearance of the epoxy samples after different times of depolymerization at 140 °C are shown in Fig. 4a (top row), and the decrease of the normalized sample mass at different temperatures are presented as dots in Fig. 4c. By fitting the simulation results to the experimental curves, we determined the scaling factor for the segment disentanglement speed (α_d in Eq. (7a)) as 0.049. This enables the FEA model to closely capture the depolymerization speeds at different temperatures (dashed lines in the figure), as well as the evolution of sample appearances in Fig. 4a (bottom row). The results in the figure also show that the alcohol solvent molecules are primarily present around the polymer-solvent interfaces. The time scale of full depolymerization (~4 h) is much shorter than that of the saturated solvent diffusion (~10 h in Fig. 3). This suggests that the network depolymerization is a faster mechanism than the solvent diffusion within the prepared epoxy samples.

With the determined disentanglement parameter, the FEA model was used to simulate the depolymerization process of the star-shaped epoxy sample. As shown in Fig. 4a and b, the shape of the epoxy samples during the depolymerization process is closely captured by the model. In addition to the high solvent content around the polymer-solvent interfaces, it is interesting to observe that the five angles of the star-shaped epoxy sample first disappear during depolymerization due to the large contact area with the solvent. The FEA model also closely captures the evolution of normalized sample mass at different depolymerization temperatures (Fig. 4d).

An epoxy material structure was prepared to further verify the efficacy of the developed FEA model to capture the essentials of the diffusion-reaction process during the epoxy depolymerization, as shown in Fig. 5a. The material structure has a cylindrical geometry with a squared cross-section. During the molding process, three glass rods are securely positioned along the longitudinal axis of the sample. This arrangement effectively emulates the influence exerted by individual carbon fibers in the depolymerization process of an actual composite material. The overall length of the structure (90 mm) is much greater than the size of the cross-section, so the depolymerization process can be taken as a 2D problem. The figure shows the appearance of the cross-section at different stages of depolymerization. The corresponding FEA simulations are also presented in the figure for comparison. It is seen that the depolymerization process is still a surface-corrosion type, and the simulation results agree with the experimental results well. The experimentally determined mass evolutions of the material structure at 120 °C and 140 °C are also closely predicted (Fig. 5b). Overall, the close comparison between experimental and simulation results in this section suggests that the developed constitutive modeling framework is efficient to capture the diffusion-reaction process and the overall depolymerization speed of epoxy samples in different configurations.

4.4. Depolymerization kinetics of epoxy composites

Influence of the fiber content and arrangements: Composite lamina samples were prepared using the vacuum-bagging process. The fiber volume contents are 19%, 33%, and 40% respectively. When applying the established FEA model to study composite depolymerization, the first challenge is to properly model the fiber arrangement. For example, the 40% composites have a thickness of ~1.6 mm. Each carbon fiber has a diameter of 7 μm. Within a 1.6 mm by 1.6 mm cross-sectional area, there would be 26,621 individual fibers. A comparable mesh size as the fiber diameter will yield millions of elements. This imposes grand challenges to mesh the model and run the simulations.

To this end, we start with a 2D FEA model with a reduced dimension (0.08 mm by 0.08 mm). Only the top side of the model is defined to be the solvent-polymer interface with diffusion and segment disentanglement boundary conditions. During realistic depolymerization of a composite sample, both top and bottom surfaces would be in contact with the solvent, so the actual depolymerization depth is half of the sample thickness (0.8 mm).This is 10 times the model height. The fibers in the FEA model are assumed to be randomly distributed without aggregates. This is realized by assigning normally distributed random numbers to define the center of the circles in the FEA model. The predicted depolymerization process of the epoxy composites with 40% carbon fiber at 140 °C is shown in Fig. 6a. It is noted that there are no parameter adjustments involved during the simulations. In the second set of reduced-order models, the fibers are placed in a neatly arranged pattern as shown in Fig. 6b, with other material parameters and identical boundary conditions. The corresponding mass changes of these two reduced-size models are plotted in the supplementary materials, Fig. S4.

First, it is observed that there is essentially no difference in the depolymerization speed of these two FEA models. Both fully

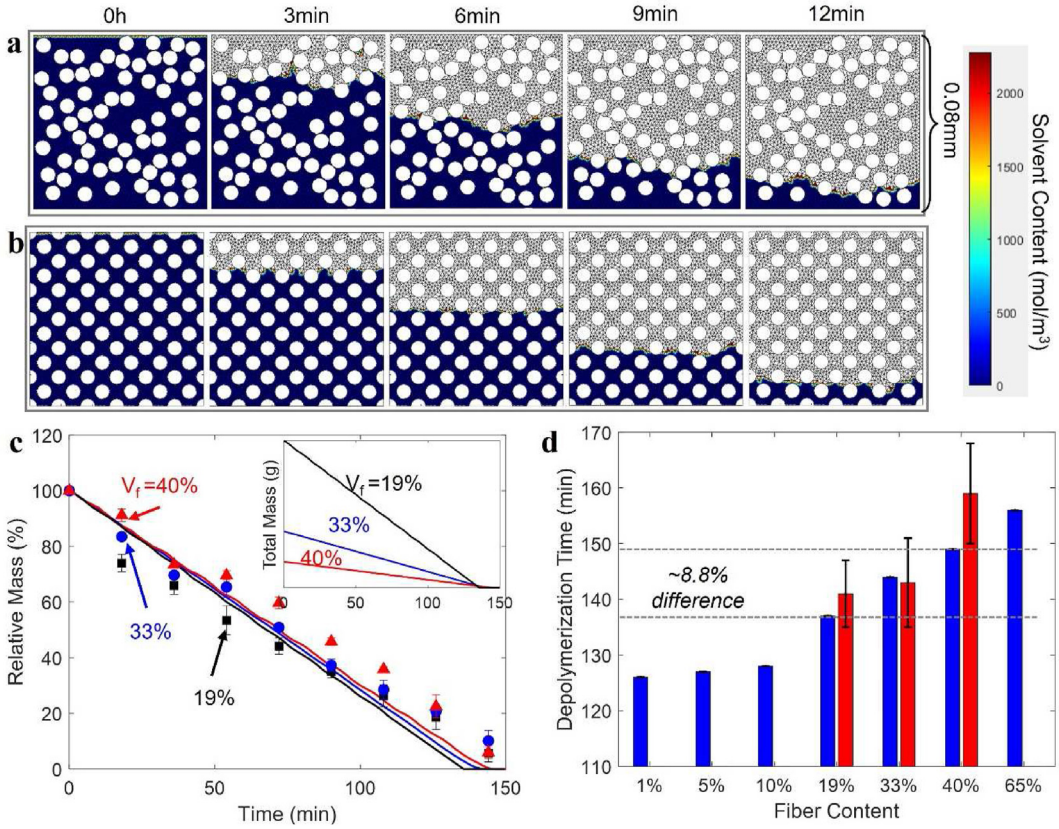

Fig. 6. The depolymerization process of the reduced-size composite model at 140 °C with 40% carbon fiber. **(a)** Randomly placed fibers. **(b)** Ordered fiber placements with same fiber content. **(c)** Decreases of normalized mass of composite samples with different fiber contents. Dots denote experimental data. Solid lines denote model predictions. **(d)** Summary of depolymerization time of composites with different fiber contents.

depolymerize at around 14.5 min. From this point of view, the randomness of fiber arrangement has a negligible influence on the composite depolymerization speed. Second, the composites depolymerize in a surface-corrosion manner. The interface between the composite and the solvent is maintained in a relatively straight profile. The overall depolymerized speed is a constant, namely, the composite mass decreases linearly as a function of time. By comparing the thicknesses of full-size composites and reduced-size models, the depolymerization time of the composite samples can be estimated to be approximately 10 times longer than that of the reduced-size model with the same mass dropping rate.

The reduced-size model with neatly arranged fibers is used to study the depolymerization of composites with different fiber contents (1%–65%). The predictions on the decrease of normalized mass are compared with experimental results in Fig. 6c. The corresponding depolymerization times are summarized in Fig. 6d. It is observed that the modeling predictions are reasonably close to the experimental data. In both the experiments and simulations, the depolymerization speed decreases with the fiber content of the composites. Since composite depolymerization is a surface-corrosion process, the overall depolymerization speed is determined by the interface between the epoxy matrix and the solvent. A higher fiber content leads to a lower contact area, and thus lowering the mass dropping rate. This can be seen from the inset view of Fig. 6c. On the other hand, the differences in the depolymerization time are much smaller compared to the differences in fiber content. For example, when the fiber content is increased from 19% to 40%, the depolymerization time is only increased by ~8.8%. The presence of a higher concentration of carbon fiber and a reduced amount of matrix in the material system leads to a reduced requirement for solvent and heating time to achieve complete depolymerization of the matrix polymer. These two mechanisms are critical to determining the final depolymerization time. The comparison in Fig. 6d also reveals that the FEA prediction on the depolymerization time of composites with 40% fiber is slightly lower than the experimental results. This might be due to the fiber aggregations that are likely present in the composites, which will be elaborated on in detail in the following section.

Influence of the depolymerization temperature and solvent diffusivity: Parametric studies are performed using the FEA model to examine the influences of temperature and solvent diffusivity on the depolymerization speed and mode. To further reduce the computational burden, representative volume element (RVE) models were created as shown in Fig. 7a. In each model, the model height and fiber content (19%) are kept constant, while the diameter of the fiber increases, leading to less amount of fiber being modeled. In RVE models (M_1-M_3), the equivalent fiber is reduced from 6 to 0.5, respectively, and the element amount is substantially reduced from ~3000 to ~600. At 140 °C, the decrease in sample mass is compared in Fig. 7b. It is seen that the time for complete depolymerization is roughly the same among different RVE models, with a maximum deviation below 2.1%. For the simplest model (RVE model M_3), it is seen that the depolymerization speed is not as constant as the others. Since composite depolymerization is shown to be a surface-corrosion type, the mass dropping rate depends on the contact area between the polymer and composites. For the simplest reduced order model, the contact area increases first and then

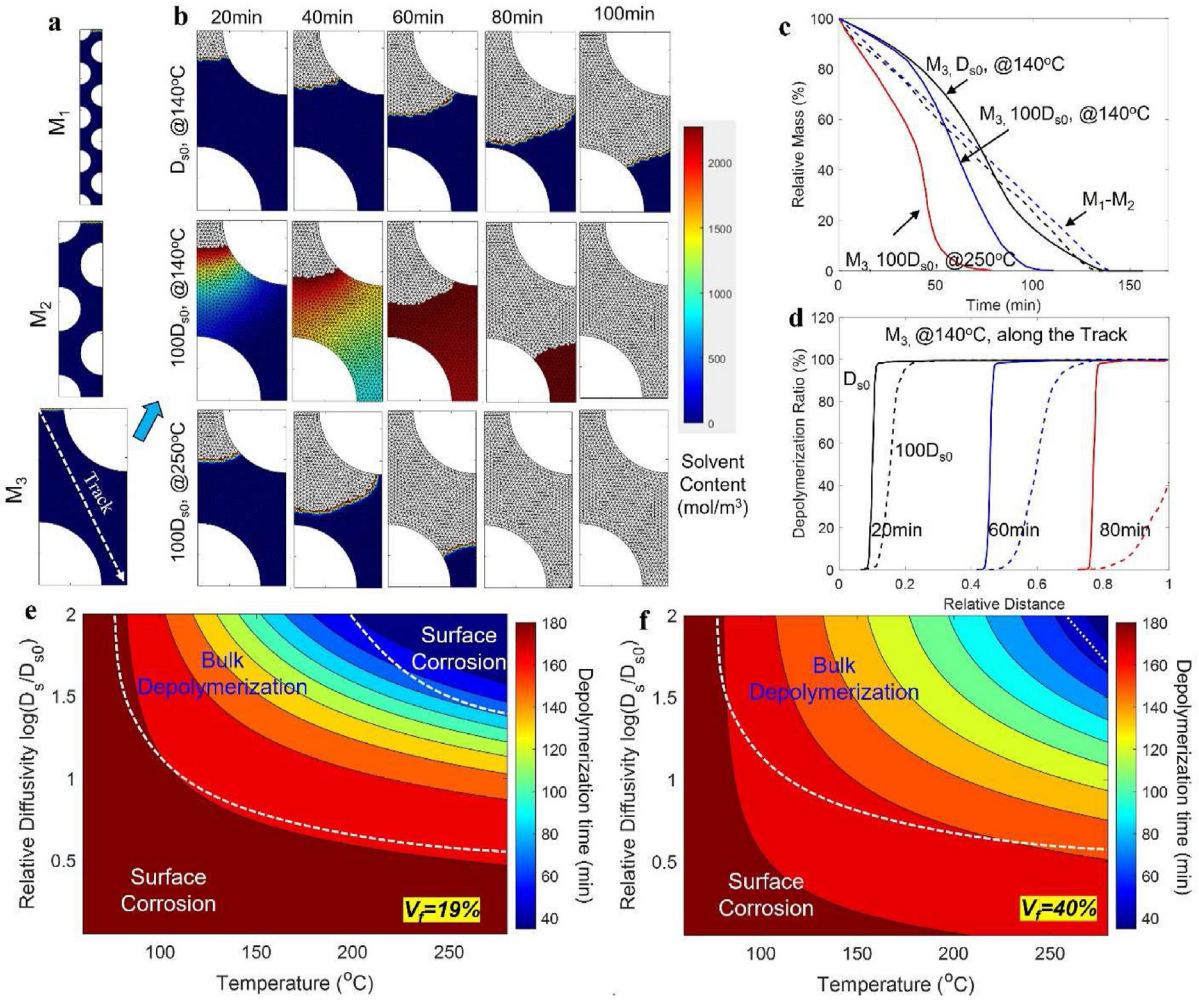

Fig. 7. **(a)** A series of RVE models with less amount of equivalent carbon fiber and a smaller number of finite elements. The height of the model and fiber content is kept constant. **(b)** The depolymerization process of the simplest RVE model with different temperatures and solvent diffusivities. **(c)** The change in the normalized mass of the composites formulated by the RVE models. **(d)** The evolution of element depolymerization ratios along the Track defined in figure a. The contour plots of the depolymerization time of epoxy composites with different temperatures and reference solvent diffusivities. The fiber contents are **(e)** 19% and **(f)** 40%, respectively.

decreases, leading to the non-uniform depolymerization profile. However, since the primary consideration during the recycling is the overall heating time, the simplest RVE model M_3 will be adopted in this section to study the influences of processing parameters on the recycling process.

To examine the influences of solvent diffusivity, the reference diffusivity D_{s0} in the FEA model is increased by 100 times, and the temperature is kept at 140 °C. In practical applications, a higher solvent diffusivity can be realized by selecting solvents with good capability (a smaller Flory-Huggins interaction parameter) with the epoxy network. Alternatively, this can be realized by mixing the alcohol solvent with a good solvent for epoxy, which swells the epoxy network quickly to allow the alcohol solvent and catalyst to quickly diffuse into the network, as shown in our previous studies and others [47,68].

The simulated depolymerization processes with $100D_{s0}$ at 140 °C are compared in Fig. 7a and c. In the meantime, the depolymerization ratio of elements along the track defined in Fig. 7a (marked with a white arrow in the M3 model) is presented in Fig. 7d. Among these curves, three solid lines represent the scenario where the solvent diffusivity is D_{s0}, while the three dashed lines correspond to a solvent diffusivity of $100D_{s0}$. Each diffusivity condition is associated with three curves, which describe the depolymerization ratio distribution at different heating times. When the depolymerization ratio reaches zero, it indicates that the elements have undergone complete depolymerization and have disappeared. As a result, these curves also serve as indicators of the solid-liquid interface position during the depolymerization process.

From the comparison, it can be observed that when solvent diffusivity is low (D_{s0}), the depolymerization ratio increases rapidly from 0 to 1, which suggests that the depolymerization is only limited around the solid-liquid interface. When the solvent diffusivity is high ($100D_{s0}$), the depolymerization ratio gradually increases with distance. This means that the network starts to be depolymerized even before the outer layer materials are completely dissolved in the liquid. The material depolymerization mode is translated from surface corrosion to bulk depolymerization, and the limiting factor for depolymerization is changed from solvent diffusivity to the rate of BERs.

The change in the depolymerization mode also affects the overall depolymerization speed of the composite sample. As shown in Fig. 7c, at the early stage of depolymerization, the mass dropping rate is close to the one with diffusivity D_{s0}. After ~50mins, the mass dropping rate increases notably, leading to a depolymerization time decrease from ~150 min to ~120 min. This is because the solvent molecules diffused inside the epoxy network actively break the

polymer chains into short segments, which exhibit a higher disentanglement rate on the polymer-solvent interface when the elements come into contact with the solvent.

In another set of simulations, the temperature for the depolymerization increased from 140 °C to 250 °C with $100D_{s0}$. The depolymerization process is compared in Fig. 7a and c. A higher processing temperature increases the rate of BERs and chain segment disentanglements, which will surpass the contribution of solvent transportation in determining the depolymerization speed. Therefore, the depolymerization mode switches back to the surface-corrosion process, with the solvent molecules primarily located around the polymer-solvent interface. The final depolymerization time of the composite sample is further reduced to ~73 min.

Parametric studies are performed using the M_3 model to predict the composite depolymerization times, which aims to provide a guideline for the design of optimal processing conditions. The solvent diffusivity increases from D_{s0} to $100D_{s0}$, and the temperature increases from 50 °C to 300 °C. Note that even though an alcohol solvent with an extremely high diffusivity for epoxy thermosets may not currently exist, the parameter studies performed provide foresight for the chemistry design and synthesis of depolymerization solvents. The simulation results are presented as contour plots in Fig. 7e and f, wherein the composite contents are 19% and 40%, respectively. For each simulation case, we also track the number of solvent molecules within the epoxy network to distinguish the depolymerization mode. If the weight of the solvent is lower than 5% of the matrix weight, the depolymerization process is taken to be a surface-corrosion process. Otherwise, it is bulk depolymerization. The readers are noted that the decision to use a 5% weight fraction for the solvent was made based on subjective criteria, primarily aimed at enabling quantitative analysis and effectively differentiating between surface corrosion and bulk depolymerization. By selecting this value, we intended to imply that the presence of solvent within the system is minimal, thereby suggesting that depolymerization predominantly takes place at the surface rather than in the bulk.

As shown in the figures, the composite depolymerization speed increases with the temperature at a given solvent diffusivity. This is because a higher temperature not only promotes solvent diffusion within the network but also accelerates the BER for chain cleavage and chain disentanglement on the polymer-solvent interface. On the other hand, for a given temperature, the depolymerization rate increases with solvent diffusivity because the solvent will diffuse faster into the network. The increased reactive small molecules promote the rates of chain cleavage and network depolymerization.

In addition, there are interesting conclusions that can be obtained from the simulations. First, the temperature is a more important parameter to determine the feasibility of composite depolymerization. Below a critical temperature of around 75 °C, the BER rate is negligible within the system, and thus, there is no depolymerization observed no matter how long the composites are heated or how high the solvent diffusivity is. Second, increasing either the temperature or the solvent diffusivity will switch the depolymerization mechanism initially from surface corrosion to bulk depolymerization, and then surface corrosion again. This results from the competition of solvent diffusivity and temperature in promoting the depolymerization speed. At a relatively low temperature or reference diffusivity, both two mechanisms are slow, and the matrix depolymerization is only limited around the polymer-solvent interfaces. As increasing the temperature, the solvent diffusivity starts to increase rapidly to enable the diffusion and network depolymerization inside the composite materials, leading to the mode of bulk depolymerization. When the temperature is higher than a critical value, the BER rate is substantially promoted. The diffused solvent molecules can quickly react with the ester bonds for chain cleavage. More solvent molecules are needed to further promote the depolymerization speed of epoxy composites. The depolymerization model returns to surface corrosion with the solvent diffusivity being the limiting factor for depolymerization speed. Third, the fiber content has a notable influence on the depolymerization speed in the bulk depolymerization domain, wherein solvent diffusion dominates the overall process. A higher fiber content blocks the transportation of solvent more significantly, and thus reduces the overall depolymerization speed. In the domains of surface corrosion, however, the influences of fiber content are less significant, because the depolymerization is only limited around the interface as revealed in the previous sections.

Influence of fiber aggregates: The previous sections assume the carbon fibers are well separated and evenly distributed within the composites. During practical composite fabrications, fiber aggregation is commonly seen and unavoidable [69–71]. First, for composites with high fiber content, individual fibers tend to attract each other due to the hydrophobic and van der Waals interactions. The presence of fiber bundles significantly impedes the transportation of solvent, thereby impacting the overall depolymerization speed of composites. As shown in Fig. 6d, the experimentally determined depolymerization time of composites with 40% carbon fiber is higher than the model predictions in the ideal cases with separated fibers. Second, for composites with low fiber content, the fiber may not be able to fully separate, especially when the fibers are woven or have fill threads held in position. There might exist a resin-rich layer and a fiber-rich layer within the composite materials [72].

To explore the influencing mechanisms of the fiber aggregates, we first created an FEA model for composites with 40% carbon fiber, as shown in Fig. 8a. The fiber aggregates are represented by circles in the FEA model with randomly assigned center positions. Each circle diameter is assigned with a uniformly distributed random number between r_0 and $6r_0$, with $r_0 = 7$ μm being the diameter of an individual fiber. The largest circle in the model represents ~36 carbon fibers associated together. The solvent transportation boundary condition is applied on the top surfaces. The depolymerization profiles shown in the figure suggest the surface-corrosion depolymerization process of the epoxy composite at 140 °C. Fig. 8b shows the decrease of composite mass with different reference diffusivities and temperatures. By increasing the solvent diffusivity by 100 times, the composite exhibits the nonlinear relationship between the sample mass and the depolymerization time, suggesting the bulk depolymerization mechanism is in play. The depolymerization time decreases from ~110 min to ~97 min. Further increasing the temperature to 250 °C promotes the BER kinetics. The nearly linear mass-time relationship indicates that the composite sample returns to the surface-corrosion depolymerization process, and the depolymerization time further reduces to ~60 min.

As a control, another FEA model with separated carbon fibers is created with the same model height and fiber content. The depolymerization profile at 140 °C and a reference diffusivity of D_{s0} is shown in Fig. 8c. The full depolymerization times in the two FEA models with different temperatures and diffusivities are summarized in Fig. 8d. The comparison shows that with a relatively low solvent diffusivity, the composites exhibit surface-corrosion depolymerization, and the difference between the two model predictions is negligible. When increasing the solvent diffusivity to enter the region of bulk depolymerization, the predictions on the depolymerization time from the M_1 aggregate FEA model are always higher than the M_2 model. After further increasing the

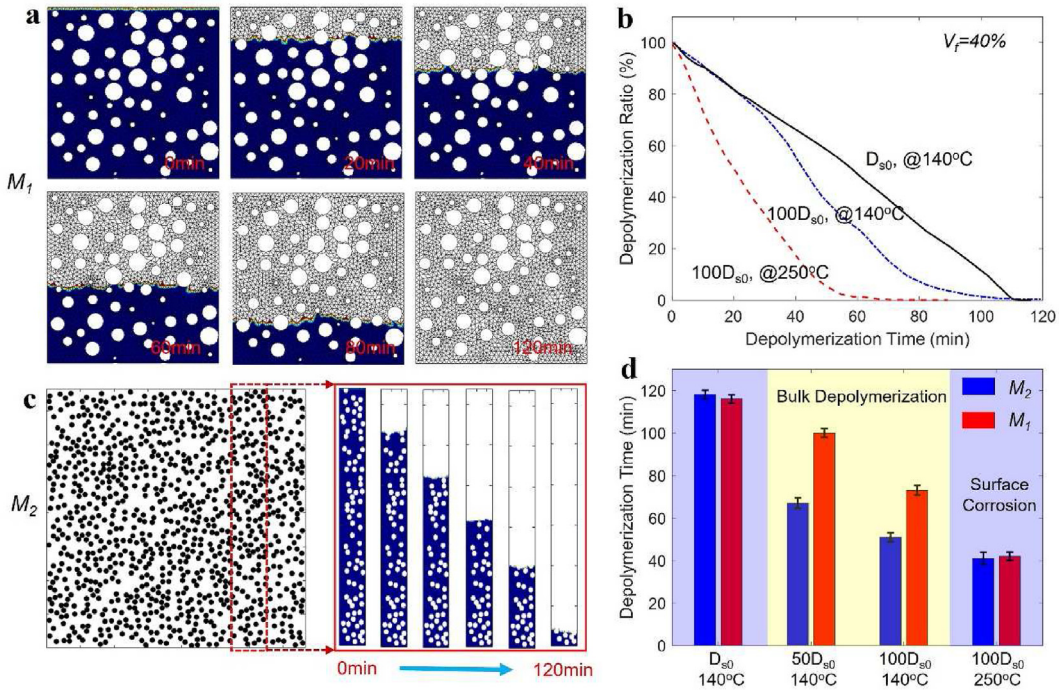

Fig. 8. **(a)** The depolymerization profile predicted by the FEA model with fiber aggregates. The temperature is 140 °C, and the fiber content is 40%. **(b)** Mass dropping as a function of time predicted by the FEA model with different fiber aggregates, temperatures, and reference solvent diffusivities. **(c)** The depolymerization profile predicted by the control FEA model with separated carbon fibers. The temperature is 140 °C and the fiber content is 40%. **(d)** Summary of the depolymerization times predicted by the two FEA models with different temperatures and reference solvent diffusivities.

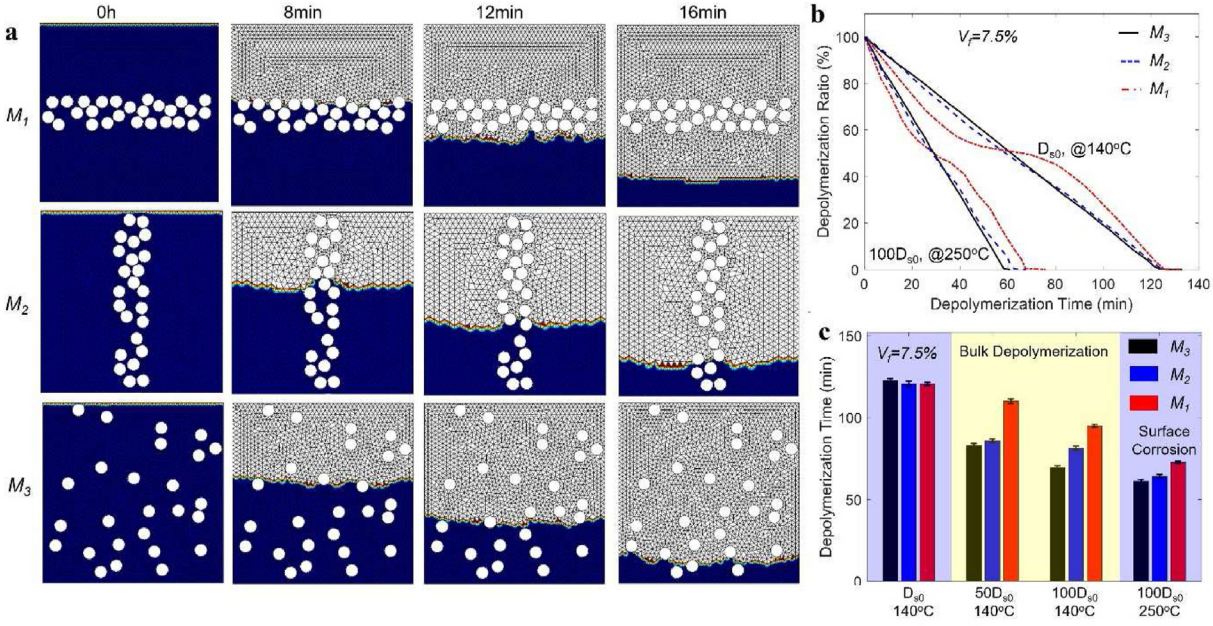

Fig. 9. **(a)** Three FEA models to study influences of fiber aggregates in composites with a lower fiber content (7.5%). The figures show the appearance of the composite cross-section as the depolymerization proceeds. **(b)** Mass dropping as a function of time predicted by the three FEA models with different temperatures and reference solvent diffusivities. **(c)** Summary of the depolymerization times predicted by the three FEA models with different temperatures and reference solvent diffusivities.

temperature, the composites return to the surface-corrosion domain, and the two models predict close depolymerization times. It is therefore concluded that the aggregates in composites with a high fiber content do not dramatically affect the overall depolymerization speed if it is in the surface-corrosion domain. Furthermore, solvent diffusivity is identified to be the limiting factor for depolymerization. However, within the bulk-depolymerization domain, solvent diffusivity is the dominating factor. The fiber aggregates notably block the diffusion of the solvent, and thus reduce the overall depolymerization speed.

To study the influences of fiber aggregates in composites with a lower fiber content (7.5%), three FEA models are created as shown

in Fig. 9a. M_1 and M_2 models have carbon fibers aggregated in a thin layer with a thickness of ~15 μm. The fiber-rich layer is respectively in the vertical and parallel direction of macroscopic solvent transportation. The M_3 model has randomly distributed and well-separated carbon fibers, serving as a control FEA model. The figure compares the predicted depolymerization profiles at 140 °C with the reference diffusivity $D_{s0} = 5.5 \times 10^{-4}$ mm^2/s. The decreases in composite mass are presented in Fig. 9b. According to the previous sections, the selected reference solvent diffusivities and temperatures enable the composite to exhibit surface-corrosion type depolymerization. It is interesting to observe that in both two processing conditions, the M_2 and M_3 FEA models exhibit an almost linear mass-time relationship due to the relatively constant contact area between the epoxy matrix and solvent. For the M_1 FEA model, the sample mass first drops at a high rate, then slows down when the corrosion interface reaches the fiber-rich layer with a smaller contact area, and eventually returns the same mass dropping rate when the fiber-rich layer is passed. On the other hand, the overall depolymerization time does not vary significantly across different models. After increasing the temperature to 250 °C and the reference diffusivity to $100D_{s0}$, all three FEA models exhibit similar depolymerization profiles with the surface-corrosion behaviors, and the depolymerization times are dramatically reduced accordingly.

The predicted depolymerization times of the three FEA models with different solvent diffusivities and temperatures are summarized in Fig. 9c. The influence of fiber aggregation is similar to that in composites with high fiber content. At processing conditions with surface-corrosion type depolymerization, the influences of fiber aggregation are less significant. However, when it is in the region of bulk polymerization, the solvent diffusivity diffusion the depolymerization process, and thus the fiber aggregates notably block the solvent transportation and matrix depolymerization. The comparison in Fig. 9c also reveals that the fiber aggregation in the M_1 FEA model, where the fiber-rich layer is vertical to the macroscopic solvent transportation direction, has a more notable blocking effect in reducing the depolymerization speed.

5. Conclusion

In this study, a physics-based multiscale computational model is defined to reveal the depolymerization mechanisms of epoxy composites embedded with continuous carbon fiber. The finite-element modeling framework links the microscale bond-exchanging kinetics to the continuum-level solvent diffusion and composite depolymerization behaviors. It shows close predictions of the swelling and depolymerization speed of the epoxy matrix with different material and processing conditions. The computational model is then used to investigate the influences of fiber arrangement on the composite depolymerization behaviors. The study reveals that as increasing either the depolymerization temperature or the solvent diffusivity, the depolymerization speed increases. The epoxy composites successively exhibit surface corrosion, then bulk depolymerization, and eventually surface corrosion-type depolymerization behaviors. Within the domain of surface-corrosion depolymerization, wherein the solvent diffusion and reaction are only limited around polymer-solvent interfaces, the fiber randomness and fiber aggregates have negligible influence on the overall depolymerization speed. A higher fiber content slightly reduces the speed due to the competition between a smaller contact area between solvent and epoxy matrix and the less amount of matrix material to depolymerize. However, within the bulk depolymerization domain, wherein the solvent can quickly diffuse inside the epoxy matrix and the depolymerization limiting factor is the reaction kinetics, the fiber aggregates notably block the diffusion of the solvent within the epoxy matrix and thus reduce the overall depolymerization speed. Overall, this study provides theoretical guidance to select optimal material and processing conditions to promote the recycling efficiency of epoxy composites wastes, which paves the way for the practical implementation of the depolymerization method in engineering applications, thereby contributing to the sustainable development of society.

Credit author statement

Chaoqian Luo: Conceptualization, Methodology, Visualization, Writing – original draft. **Christopher Chung:** Investigation, Visualization, Writing – original draft. **Kai Yu:** Conceptualization, Writing – review & editing, Supervision, Project administration, Funding acquisition.

Declaration of competing interest

The authors declare the following financial interests/personal relationships which may be considered as potential competing interests:

Kai Yu reports financial support was provided by National Science Foundation.

Data availability

Data will be made available on request.

Acknowledgments

K.Y. acknowledges the support from the National Science Foundation (grant CMMI-1901807).

Appendix A. Supplementary data

Supplementary data to this article can be found online at https://doi.org/10.1016/j.mtsust.2023.100452.

References

[1] D. Chung, Carbon Fiber Composites, Butterworth-Heinemann, 2012.
[2] P. Morgan, Carbon Fibers and Their Composites, CRC Press, 2005.
[3] V.P. McConnell, Launching the carbon fibre recycling industry, Reinforc. Plast. 54 (2) (2010) 33–37.
[4] F.R. Meng, J. McKechnie, T. Turner, K.H. Wong, S.J. Pickering, Environmental aspects of use of recycled carbon fiber composites in automotive applications, Environ. Sci. Technol. 51 (21) (2017) 12727–12736.
[5] T. Ghosh, H.C. Kim, R. De Kleine, T.J. Wallington, B.R. Bakshi, Life cycle energy and greenhouse gas emissions implications of using carbon fiber reinforced polymers in automotive components: front subframe case study, Sustain. Mater. Technol. 28 (2021).
[6] F. Meng, J. McKechnie, T.A. Turner, S.J. Pickering, Energy and environmental assessment and reuse of fluidised bed recycled carbon fibres, Compos. Appl. Sci. Manuf. 100 (2017) 206–214.
[7] X. Li, R.B. Bai, J. McKechnie, Environmental and financial performance of mechanical recycling of carbon fibre reinforced polymers and comparison with conventional disposal routes, J. Clean. Prod. 127 (2016) 451–460.
[8] P.T. Williams, A. Cunliffe, N. Jones, Recovery of value-added products from the pyrolytic recycling of glass-fibre-reinforced composite plastic waste, J. Energy Inst. 78 (2) (2005) 51–61.
[9] R.E. Allred, Recycling process for scrap composites and prepregs, SAMPE J. 32 (5) (1996) 46–51.
[10] R.E. Allred, A.B. Coons, R.J. Simonson, Properties of carbon fibers reclaimed from composite manufacturing scrap by tertiary recycling, Technol. Trans. Global Commun. 28 (1996) 139–150.
[11] R.E. Allred, J.M. Gosau, J.M. Shoemaker, Recycling process for carbon/epoxy composites, in: 2001: A Materials and Processes Odyssey, Books 1 and 2, vol. 46, 2001, pp. 179–192.
[12] G. Jiang, S.J. Pickering, G.S. Walker, N. Bowering, K.H. Wong, C.D. Rudd, Soft ionisation analysis of evolved gas for oxidative decomposition of an epoxy resin/carbon fibre composite, Thermochim. Acta 454 (2) (2007) 109–115.

[13] H.L.H. Yip, S.J. Pickering, C.D. Rudd, Characterisation of carbon fibres recycled from scrap composites using fluidised bed process, Plast. Rubber Compos. 31 (6) (2002) 278–282.
[14] B.J. Jody, E.J. Daniels, F.L. Paulauskas, M.G. Abdallah, A process to recover carbon fibres from polymer matrix composite scrap, Int. SAMPE Symp. Exhib. 49 (2004) 35–47.
[15] M.S. Qureshi, A. Oasmaa, H. Pihkola, I. Deviatkin, A. Tenhunen, J. Mannila, H. Minkkinen, M. Pohjakallio, J. Laine-Ylijoki, Pyrolysis of plastic waste: opportunities and challenges, J. Anal. Appl. Pyrol. 152 (2020).
[16] I. Vollmer, M.J.F. Jenks, M.C.P. Roelands, R.J. White, T. van Harmelen, P. de Wild, G.P. van der Laan, F. Meirer, J.T.F. Keurentjes, B.M. Weckhuysen, Beyond mechanical recycling: giving new life to plastic waste, Angew. Chem. Int. Ed. 59 (36) (2020) 15402–15423.
[17] Y.Q. Wang, X.J. Cui, Q.Q. Yang, T.S. Deng, Y.X. Wang, Y.X. Yang, S.Y. Jia, Z.F. Qin, X.L. Hou, Chemical recycling of unsaturated polyester resin and its composites via selective cleavage of the ester bond, Green Chem. 17 (9) (2015) 4527–4532.
[18] T. Liu, M. Zhang, X.L. Guo, C.Y. Liu, T. Liu, J.N. Xin, J.W. Zhang, Mild chemical recycling of aerospace fiber/epoxy composite wastes and utilization of the decomposed resin, Polym. Degrad. Stabil. 139 (2017) 20–27.
[19] A.D. La Rosa, D.R. Banatao, S.J. Pastine, A. Latteri, G. Cicala, Recycling treatment of carbon fibre/epoxy composites: materials recovery and characterization and environmental impacts through life cycle assessment, Compos. B Eng. 104 (2016) 17–25.
[20] B.J. Adzima, H.A. Aguirre, C.J. Kloxin, T.F. Scott, C.N. Bowman, Rheological and chemical analysis of reverse gelation in a covalently cross-linked diels-alder polymer network, Macromolecules 41 (23) (2008) 9112–9117.
[21] M.A. Tasdelen, Diels–Alder "click" reactions: recent applications in polymer and material science, Polym. Chem. 2 (2011) 2133–2145.
[22] C.J. Kloxin, T.F. Scott, B.J. Adzima, C.N. Bowman, Covalent adaptable networks (CANS): a unique paradigm in cross-linked polymers, Macromolecules 43 (6) (2010) 2643–2653.
[23] C.N. Bowman, C.J. Kloxin, Covalent adaptable networks: reversible bond structures incorporated in polymer networks, Angew. Chem. Int. Ed. 51 (18) (2012) 4272–4274.
[24] R.J. Wojtecki, M.A. Meador, S.J. Rowan, Using the dynamic bond to access macroscopically responsive structurally dynamic polymers, Nat. Mater. 10 (1) (2011) 14–27.
[25] Z. Lei, H. Chen, C. Luo, Y. Rong, Y. Hu, Y. Jin, R. Long, K. Yu, W. Zhang, Recyclable and malleable thermosets enabled by activating dormant dynamic linkages, Nat. Chem. 14 (12) (2022) 1399–1404.
[26] C. Luo, Z. Lei, Y. Mao, X. Shi, W. Zhang, K. Yu, Chemomechanics in the moisture-induced malleability of polyimine-based covalent adaptable networks, Macromolecules 51 (23) (2018) 9825–9838.
[27] P. Taynton, K. Yu, R.K. Shoemaker, Y. Jin, H.J. Qi, W. Zhang, Heat-or water-driven malleability in a highly recyclable covalent network polymer, Adv. Mater. 26 (23) (2014) 3938–3942.
[28] L. Zhong, Y. Hao, J. Zhang, F. Wei, T. Li, M. Miao, D. Zhang, Closed-loop recyclable fully bio-based epoxy vitrimers from ferulic acid-derived hyperbranched epoxy resin, Macromolecules 55 (2) (2022) 595–607.
[29] J. Zhang, Z. Gong, C. Wu, T. Li, Y. Tang, J. Wu, C. Jiang, M. Miao, D. Zhang, Itaconic acid-based hyperbranched polymer toughened epoxy resins with rapid stress relaxation, superb solvent resistance and closed-loop recyclability, Green Chem. 24 (18) (2022) 6900–6911.
[30] L.M. Johnson, E. Ledet, N.D. Huffman, S.L. Swarner, S.D. Shepherd, P.G. Durham, G.D. Rothrock, Controlled degradation of disulfide-based epoxy thermosets for extreme environments, Polymer 64 (2015) 84–92.
[31] A.R.d. Luzuriaga, R. Martin, N. Markaide, A. Rekondo, G. Cabañero, J.R.a.I. Odriozola, Epoxy resin with exchangeable disulfide crosslinks to obtain reprocessable, repairable and recyclable fiber-reinforced thermoset composites, Mater. Horiz. 3 (2016) 241–247.
[32] D.W. Hanzon, N.A. Traugutt, M.K. McBride, C.N. Bowman, C.M. Yakacki, K. Yu, Adaptable liquid crystal elastomers with transesterification-based bond exchange reactions, Soft Matter 14 (6) (2018) 951–960.
[33] P. Taynton, H.G. Ni, C.P. Zhu, K. Yu, S. Loob, Y.H. Jin, H.J. Qi, W. Zhang, Repairable woven carbon fiber composites with full recyclability enabled by malleable polyimine networks, Adv. Mater. 28 (15) (2016) 2904–2909.
[34] X. He, Z. Lei, W. Zhang, K. Yu, Recyclable 3D printing of polyimine-based covalent adaptable network polymers, 3D Print. Addit. Manuf. 6 (1) (2019) 31–39.
[35] X. He, X. Shi, C. Chung, Z. Lei, W. Zhang, K. Yu, A sustainable manufacturing method of thermoset composites based on covalent adaptable network polymers, Compos. B Eng. 221 (2021) 109004.
[36] X. He, Y. Lin, Y. Ding, A.M. Abdullah, Z. Lei, Y. Han, X. Shi, W. Zhang, K. Yu, Reshapeable, rehealable and recyclable sensor fabricated by direct ink writing of conductive composites based on covalent adaptable network polymers, Int. J. Extrem. Manuf. 4 (1) (2021) 015301.
[37] K. Yu, Q. Shi, M.L. Dunn, T.J. Wang, H.J. Qi, Carbon fiber reinforced thermoset composite with near 100% recyclability, Adv. Funct. Mater. 26 (33) (2016) 6098–6106.
[38] Q. Shi, K. Yu, M.L. Dunn, T.J. Wang, H.J. Qi, Solvent assisted pressure-free surface welding and reprocessing of malleable epoxy polymers, Macromolecules 49 (15) (2016) 5527–5537.
[39] X. Shi, C. Luo, H. Lu, K. Yu, Primary recycling of anhydride-cured engineering epoxy using alcohol solvent, Polym. Eng. Sci. 59 (s2) (2019) E111–E119.
[40] Q. Shi, K. Yu, X. Kuang, X.M. Mu, C.K. Dunn, M.L. Dunn, T.J. Wang, H.J. Qi, Recyclable 3D printing of vitrimer epoxy, Mater. Horiz. 4 (4) (2017) 598–607.
[41] X. Shi, C. Luo, H. Lu, K. Yu, Interfacial welding and reprocessing of engineering thermosets based on surface depolymerization, Surf. Interf. 26 (2021) 101368.
[42] X. Shi, D. Soule, Q. Ge, H. Lu, K. Yu, Evolution of material properties during the solvent-assisted recycling of thermosetting polymers: to reduce the residual stress and material inhomogeneity, Mater. Today Sustain. 19 (2022) 100167.
[43] C. Luo, B. Zhang, W. Zhang, C. Yuan, M. Dunn, Q. Ge, K. Yu, Chemomechanics of dual-stage reprocessable thermosets, J. Mech. Phys. Solids 126 (2019) 168–186.
[44] K. Yu, H. Yang, B.H. Dao, Q. Shi, C.M. Yakacki, Dissolution of covalent adaptable network polymers in organic solvent, J. Mech. Phys. Solids 109 (2017) 78–94.
[45] F.I. Altuna, C.E. Hoppe, R.J. Williams, Epoxy vitrimers with a covalently bonded tertiary amine as catalyst of the transesterification reaction, Eur. Polym. J. 113 (2019) 297–304.
[46] X. Bories-Azeau, S.P. Armes, Unexpected transesterification of tertiary amine methacrylates during methanolic ATRP at ambient temperature: a cautionary tale, Macromolecules 35 (27) (2002) 10241–10243.
[47] X. Kuang, Y.Y. Zhou, Q. Shi, T.J. Wang, H.J. Qi, Recycling of epoxy thermoset and composites via good solvent assisted and small molecules participated exchange reactions, ACS Sustain. Chem. Eng. 6 (7) (2018) 9189–9197.
[48] S.A. Lima, M. Kamrujjaman, M.S. Islam, Numerical solution of convection-diffusion-reaction equations by a finite element method with error correlation, AIP Adv. 11 (8) (2021).
[49] Z. Gharibi, M. Dehghan, Convergence analysis of weak Galerkin flux-based mixed finite element method for solving singularly perturbed convection-diffusion-reaction problem, Appl. Numer. Math. 163 (2021) 303–316.
[50] R.C. Lin, X. Ye, S.Y. Zhang, P. Zhu, A weak Galerkin finite element method for singularly perturbed convection-diffusion-reaction problems, SIAM J. Numer. Anal. 56 (3) (2018) 1482–1497.
[51] G.R. Barrenechea, A.H. Poza, H. Yorston, A stabilised finite element method for the convection-diffusion-reaction equation in mixed form, Comput. Methods Appl. Mech. Eng. 339 (2018) 389–415.
[52] C.M. Hamel, X. Kuang, H.J. Qi, Modeling the dissolution of thermosetting polymers and composites via solvent assisted exchange reactions, Compos. B Eng. (2020) 200.
[53] M. Valentini, H. Rüegger, P.S. Pregosin, Applications of Pulsed-Gradient Spin-Echo (PGSE) diffusion measurements in organometallic chemistry, Helv. Chim. Acta 84 (10) (2001) 2833–2853.
[54] H.C. Chen, S.H. Chen, Diffusion of crown ethers in alcohols, J. Phys. Chem. 88 (21) (1984) 5118–5121.
[55] A. Polson, The some aspects of diffusion in solution and a definition of a colloidal particle, J. Phys. Chem. 54 (5) (1950) 649–652.
[56] R. Evans, Z. Deng, A.K. Rogerson, A.S. McLachlan, J.J. Richards, M. Nilsson, G.A. Morris, Quantitative interpretation of diffusion-ordered NMR spectra: can we rationalize small molecule diffusion coefficients? Angew. Chem. Int. Ed. 52 (11) (2013) 3199–3202.
[57] A. Macchioni, G. Ciancaleoni, C. Zuccaccia, D. Zuccaccia, Determining accurate molecular sizes in solution through NMR diffusion spectroscopy, Chem. Soc. Rev. 37 (3) (2008) 479–489.
[58] J. Duda, J. Vrentas, S. Ju, H. Liu, Prediction of diffusion coefficients for polymer-solvent systems, AIChE J. 28 (2) (1982) 279–285.
[59] J. Duda, Molecular diffusion in polymeric systems, Pure Appl. Chem. 57 (11) (1985) 1681–1690.
[60] T. Lindvig, M.L. Michelsen, G.M. Kontogeorgis, A Flory–Huggins model based on the Hansen solubility parameters, Fluid Phase Equil. 203 (1–2) (2002) 247–260.
[61] A. Pathania, R.K. Arya, S. Ahuja, Crosslinked polymeric coatings: preparation, characterization, and diffusion studies, Prog. Org. Coat. 105 (2017) 149–162.
[62] V.V. Krongauz, Diffusion in polymers dependence on crosslink density, J. Therm. Anal. Calorim. 102 (2) (2010) 435–445.
[63] D.S. Clague, R.J. Phillips, Hindered diffusion of spherical macromolecules through dilute fibrous media, Phys. Fluids 8 (7) (1996) 1720–1731.
[64] M. Rubinstein, R.H. Colby, Polymer Physics, vol. 23, Oxford University Press, New York, 2003.
[65] X. Shi, D. Soule, Y. Mao, C. Yakacki, H. Lu, K. Yu, A multiscale chemomechanics theory for the solvent–assisted recycling of covalent adaptable network polymers, J. Mech. Phys. Solids 138 (2020) 103918.
[66] D.I. Bower, An Introduction to Polymer Physics, Cambridge University Press, Cambridge, 2002, p. 444.
[67] M. Rubinstein, R.H. Colby, Polymer Physics, Oxford University Press, New York, 2003.
[68] X.J. Shi, X. He, C.Q. Luo, C.S.P. Chung, Y.C. Ding, K. Yu, Influences of material and processing conditions on the depolymerization speed of anhydride-cured epoxy during the solvent-assisted recycling, Polymer (2022) 252.
[69] G. Barra, L. Guadagno, B. Simonet, B. Santos, The influence of different dispersion methods on the size of the aggregate of CNTs in epoxy resin for the manufacturing of carbon fiber reinforced composites, in: Viii International

Conference on Times of Polymers and Composites: From Aerospace to Nanotechnology, 2016, p. 1736.
[70] A. Godara, L. Mezzo, F. Luizi, A. Warrier, S.V. Lomov, A.W. van Vuure, L. Gorbatikh, P. Moldenaers, I. Verpoest, Influence of carbon nanotube reinforcement on the processing and the mechanical behaviour of carbon fiber/epoxy composites, Carbon 47 (12) (2009) 2914–2923.
[71] F.H. Gojny, M.H.G. Wichmann, B. Fiedler, K. Schulte, Influence of different carbon nanotubes on the mechanical properties of epoxy matrix composites – a comparative study, Compos. Sci. Technol. 65 (15–16) (2005) 2300–2313.
[72] Mechanical performance of carbon-epoxy laminates part I: quasi-static and impact bending properties, Mater. Res. 9 (2) (2006) 115–120.